Journal of Catalysis **206,** 49–59 (2002)
doi:10.1006/jcat.2001.3473, available online at http://www.idealibrary.com on IDEAL®

Oxidative Dehydrogenation of Propane over Vanadia–Magnesia Catalysts Prepared by Thermolysis of $OV(O^tBu)_3$ in the Presence of Nanocrystalline MgO

Chanho Pak, Alexis T. Bell,[1] and T. Don Tilley[1]

Chemical Sciences Division, Lawrence Berkeley National Laboratory and Department of Chemistry and Department of Chemical Engineering, University of California, Berkeley, Berkeley, California 94720-1462

Received May 21, 2001; revised November 20, 2001; accepted November 20, 2001

The influence of vanadium content on the performance of V–Mg–O catalysts for the oxidative dehydrogenation (ODH) of propane was investigated. High-surface-area (380 m^2/g) MgO was prepared by hydrolysis of $Mg(OCH_3)_2$ followed by hypercritical drying. Vanadia was deposited on this support by thermolysis of $OV(O^tBu)_3$. Catalysts prepared by this means have BET surface areas of 187–299 m^2/g and apparent surface densities of V_2O_5 of 1.1–10.3 VO_x/nm^2. All of the catalysts were characterized by X-ray diffraction, temperature-programmed reduction, and Raman, UV–visible, and nuclear magnetic resonance spectroscopy. The environment of the V atoms depends strongly on the apparent surface density of vanadia. Isolated VO_4^{2-} units are present at very low apparent surface densities ($\sim$1 VO_x/nm^2). As the vanadia density increases, magnesium vanadate structures are formed and above a surface density of 3.5 VO_x/nm^2 well-dispersed magnesium orthovanadate domains become evident. The rate of ODH per V atom increases with increasing VO_x surface density and reaches a maximum value at 3.5 VO_x/nm^2. Above this surface density, the rate of ODH per V atom decreases because an increasing fraction of the V atoms lie below the catalyst surface and, hence, are inaccessible. Consistent with this interpretation, the ODH activity per unit surface area reaches a plateau at a VO_x surface density of about 4 VO_x/nm^2. The propane ODH selectivity of the catalysts increases with increasing VO_x surface density and reaches a plateau of 80% for an apparent surface density of about 4 VO_x/nm^2. Rate coefficients for propane ODH (k_1), propane combustion (k_2), and propene combustion (k_3) were calculated for each catalyst. The value of k_1 increases with increasing VO_x surface density, reaching a maximum at about 4 VO_x/nm^2. By contrast, the ratios (k_2/k_1) and (k_3/k_1) decrease monotonically with increasing VO_x surface density. The observed trends in k_1, (k_2/k_1), and (k_3/k_1) are discussed in terms of the surface structure of the catalyst.

INTRODUCTION

Considerable effort has been devoted to the identification of catalysts for the oxidative dehydrogenation of propane to propene (1–6). These studies have demonstrated that the most promising candidates contain vanadia and that the activity and selectivity of such catalysts depends on the local composition and structure of the vanadium-containing species present at the catalyst surface. Investigations of catalyst structure have shown that the local environment of vanadium atoms can be a strong function of the catalyst support and the vanadia loading (1–37). Vanadia supported on oxides such as SiO_2, Al_2O_3, TiO_2, and ZrO_2 is generally present as isolated vanadyl species, polymeric vanadate species, and small particles of V_2O_5. By contrast, when vanadia is supported on basic oxides such as CaO, MgO, and so forth, metal vanadates are readily formed.

Particular attention has been given to V–Mg–O catalysts since they exhibit relatively high propene selectivities at zero propane conversion ($\sim$80%) and a lower loss in propene selectivity with increasing propane conversion than is observed for other vanadium-containing catalysts (18–37). Structural investigations of V–Mg–O catalysts show no evidence for either isolated vanadyl or polymeric vanadate species, or crystallites of V_2O_5. Instead, as the vanadia loading increases, first isolated tetrahedral VO_4 units and then stoichiometric magnesium vanadates are observed, the latter being principally magnesium orthovanadate [$Mg_3(VO_4)_2$] with smaller amounts of magnesium pyrovanadate [$Mg_2V_2O_7$]. Since the intrinsic propene selectivity at zero propene conversion increases with increasing vanadia loading, it has been proposed that the high initial propene selectivity observed for V–Mg–O catalysts is attributable to the presence of magnesium vanadate phases. While there has been some debate as to whether $Mg_3(VO_4)_2$ or $Mg_2V_2O_7$ is more selective, comparison of propene selectivity–conversion curves for these phases from different authors suggests that the two are very similar (27). It has also been noted that synergies between magnesium vanadate and magnesia lead to higher propene selectivities than are observed for pure magnesium vanadate phases (27). By contrast to what is known about the selectivity of V–Mg–O catalysts, relatively little has been

[1] To whom correspondence should be addressed. E-mail: bell@cchem.berkeley.edu; tilley@cchem.berkeley.edu.

0021-9517/02 $35.00

reported on the influence of vanadia loading on the activity of such catalysts. Likewise, nothing is known concerning the effects of catalyst structure on the rate coefficients for oxidative dehydrogenation, propane combustion, and propene combustion compared to what has been reported for vanadia supported on various oxides (13, 14).

In the present study, high-surface-area V–Mg–O catalysts were obtained by a novel synthetic route. Nanocrystalline magnesia was prepared in a manner previously described by Klabunde and coworkers (38–40) and then contacted with a molecular precursor, $OV(O^tBu)_3$, dissolved in a nonpolar organic solvent. The active form of the catalyst is formed by thermolysis of the precursor. In related work, we have shown that a similar approach leads to well-defined vanadia–zirconia catalysts that exhibit enhanced selectivities and activities for the oxidative dehydrogenation (ODH) of propane (41–45). These improved properties are associated with higher surface areas and better dispersion of the catalytically active material, relative to more traditional routes based on aqueous impregnation methods. In the present work, we have examined the effects of vanadia loading on the activity and selectivity of V–Mg–O catalysts for the oxidative dehydrogenation of propane to propene. The structure and properties of the catalysts were characterized by X-ray diffraction, by Raman, UV–visible, and ^{51}V NMR spectroscopy, and by temperature-programmed reduction. Catalyst activity and selectivity are interpreted in terms of the apparent first-order rate coefficients for the oxidative dehydrogenation of propane, the combustion of propane, and the combustion of propene.

EXPERIMENTAL

High-surface-area $Mg(OH)_2$ was prepared using a modification of the method reported in Ref. (40). A methanol solution containing 10 wt% $Mg(OCH_3)_2$ was produced by dissolving 5 g of Mg turnings (Fisher) washed with dilute HCl solution in 205 ml of methanol overnight with stirring. Hydrolysis of $Mg(OCH_3)_2$ to form dispersed $Mg(OH)_2$ was performed by adding deionized water (2 ml) dropwise into a stirred mixture of the methanol solution (20 ml) described above and 160 ml of toluene. This magnesium hydroxide gel solution was transferred into a glass liner and placed inside a 2-L Parr high-pressure autoclave. After flushing with N_2 for 5 min, the reactor was pressurized to 100 psi with N_2. The temperature of the reactor was increased to 538 K over 30 min and maintained at this temperature for 10 min before venting the gas to release the pressure, which had increased to 400 psi. The reactor was flushed with N_2 for 10 min and allowed to cool to room temperature. The white solid product ($Mg(OH)_2$) was removed from the reactor and dried in an oven at 383 K for several hours. This material was converted into MgO by heating in flowing He while the temperature was raised to 493 K at 1 K/min. The temperature was then maintained at 493 K, after which it was raised to 773 K at 1 K/min and held at this temperature for 5 h.

The vanadium precursor $OV(O^tBu)_3$ was synthesized by reaction of V_2O_5 (Aldrich) with ^{t}BuOH in benzene (46). The preparation of this compound was carried out in an inert atmosphere using a Schlenk line. Twenty grams of V_2O_5 was first placed in a 1-L round-bottom flask and connected to a Dean–Stark trap to capture the water from the reaction and the reflux condenser. After adding 300-ml of benzene, 165 ml of ^{t}BuOH was added to the benzene suspension of V_2O_5. The temperature was increased to ca. 368 K and maintained overnight. After reaction, the color of the solution changed to orange from red. The solution was filtered away from unreacted V_2O_5. After removing the solvent by distillation, white crystals were observed. This product was further dried overnight under reduced pressure. To purify the freshly formed product ($OV(O^tBu)_3$), sublimation was conducted under vacuum at 313 K. After purification, the compound was identified by the presence of a strong ^1H NMR resonance at 1.44 ppm.

V–Mg–O catalysts were prepared by impregnation of MgO with a toluene solution of $OV(O^tBu)_3$ in a manner related to a method reported in the literature (47). After transferring a syringe containing the solution of $OV(O^tBu)_3$ from a glove box, the solution was added with stirring to the MgO placed inside a 100-ml Schlenk round-bottom flask. After 1 h of stirring, the toluene was removed by evaporation under vacuum. Calcination of the catalyst was performed by heating to 823 K at 1 K/min and holding for 6 h in a flow of air. The samples were labeled nV–Mg–O, where n is the nominal weight percentage of V_2O_5 in the sample.

Powder X-ray diffraction (XRD) patterns were recorded at room temperature using a Siemens D5000 diffractometer (Cu $K\alpha$, $\lambda = 0.15406$ nm, 45 kV, 35 mA). Values of 2θ between 20 and 80° were scanned with a step size of 0.05°. The calcined catalyst powder was spread out on a borosilicate disk (by pressing a small spatula) and then loaded into the diffractometer. The patterns were corrected for any borosilicate background. Nitrogen adsorption–desorption isotherms were measured at 77 K with a static volumetric instrument (Autosorb-1, Quantachrome) after degassing the sample at 393 K for longer than 5 h under vacuum.

Raman spectra were obtained using a HoloLab Series 5000 Raman spectrometer (Kaiser Optical) equipped with an Nd YAG laser frequency doubled to 532 nm. The catalyst was pressed into a wafer around 0.1-cm thick and 0.9-cm diameter and then placed within a quartz cell. The laser was operated at a power level of 75 mW. The Raman spectrum was recorded after treating the sample at 773 K in a He flow for 1 h and cooling it to room temperature.

Diffuse reflectance UV–visible (DR–UV–vis) spectra were recorded using a Varian–Cary 4 spectrophotometer equipped with a Harrick diffuse reflectance attachment. MgO was used as a reference. Reflectance measurements

were converted to absorption spectra using the Kubelka–Munk function. UV–visible spectra were measured in the range of 1.5–50 eV at room temperature.

Solid-state ^{51}V NMR spectra were acquired on a home-built spectrometer with a field strength of 9 T (370 MHz resonance frequency for ^{1}H). The static, wide-line spectra were obtained at room temperature with samples sealed in 20- to 30-mm long, 5-mm diameter NMR tubes under vacuum using a single pulse sequence (pulse angle, 2 μs; delay time, 100 ms; spectral width, 500 kHz; line broadening, 100 Hz; 10^4–10^7 scans). A vacuum-sealed sample of neat $VOCl_3$ was used as an external reference.

Reduction rates of VO_x were measured using a modified Quantasorb surface area analyzer (Quantachrome). Samples were heated in a 20% H_2/Ar mixture (80 cm^3/min, Matheson UHP, certified mixture). The H_2 concentration in the effluent was measured by a thermal conductivity detector after removal of water in a trap containing 13× molecular sieves. Samples were held in a 4-mm I.D. quartz cell containing a quartz thermowell directly in contact with the sample. The amount of catalyst in these experiments was adjusted so that the equivalent of 3 mg of V_2O_5 was used for all measurements. The H_2 concentration in the gas flow was measured as the temperature was increased at 10 K/min to 900 K. The thermal conductivity response was calibrated using the complete reduction of CuO (Aldrich).

Rates of reaction and selectivities for the oxidative dehydrogenation of propane were measured in a fixed-bed quartz reactor using 15 mg of catalyst diluted with quartz powder (0.50 g; particle size, 0.246–0.495 mm) to prevent temperature gradients. A mixture of propane (25 cm^3/min), oxygen (9 cm^3/min), and nitrogen (2 cm^3/min) in He (200 cm^3/min) was introduced into the reactor at controlled flow rates. The gaseous reactants and products were analyzed online with a Hewlett–Packard 6890 gas chromatograph equipped with both a capillary column (HP-1) and a packed column (HAYESEP-Q). Only C_3H_6, CO, CO_2, and H_2O were observed as products. The conversion of propane was measured at total flow rates of 60–235 cm^3/min and reaction temperatures of 673, 723, and 773 K.

RESULTS AND DISCUSSION

Catalyst Structure

The product obtained by hypercritical drying of the magnesium hydroxide gel exhibits XRD peaks at 37 and 59° that are characteristic of the (101) and (110) lines of $Mg(OH)_2$. The BET surface area of this material is 1100 m^2/g. Heating in flowing He at 773 K reduces the BET surface area to 380 m^2/g and two very broad peaks centered at 43 and 62° corresponding to the (200) and (220) diffraction lines of MgO appear in the XRD pattern (48, 49). The size of the MgO particles, estimated from the Scherrer equation using the width of the peak at 62°, is 4.4 nm.

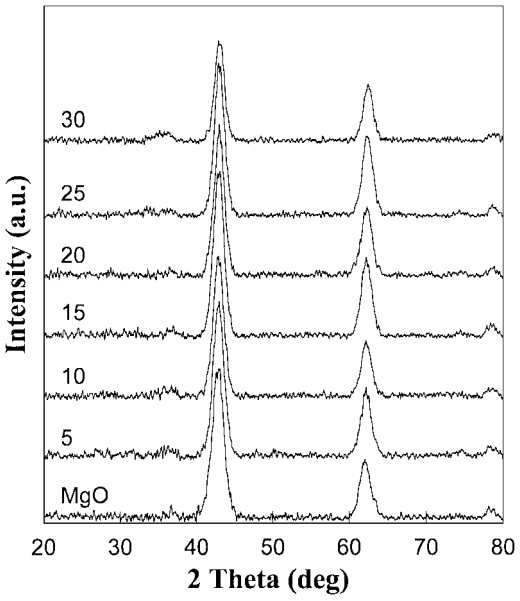

FIG. 1. Powder X-ray diffraction patterns of MgO and V–Mg–O catalysts with different V_2O_5 loadings.

Figure 1 shows XRD patterns for the V–Mg–O materials after calcination at 823 K. All of the samples show two peaks attributable to MgO and no evidence for V_2O_5. In the case of the sample containing 30 wt% V_2O_5, a broad band appears between 30 and 40°. Similar features have been reported previously and have been attributed to partially crystallized Mg orthovanadate (27, 30, 50). As the loading of vanadia increases from 5 to 30 wt%, the BET surface area decreases from 307 to 187 m^2/g and the apparent surface density of VO_x, assuming all of the vanadium is exposed on the surface, increases from 1.1 to 10.6 VO_x/nm^2 (see Table 1). The observed decrease in surface area with increasing vanadia loading is similar to that reported previously for V–Mg–O catalysts prepared by aqueous impregnation of $Mg(OH)_2$ with NH_4VO_3 and subsequent calcination (19, 22, 25).

Raman spectra of the V–Mg–O catalyst calcined at 823 K are shown in Fig. 2. Between 5 and 15 wt% V_2O_5, only one relatively narrow peak is observed, at around 825 cm^{-1}. This peak can be assigned to V–O–M (M = Mg or V) vibrations of tetrahedrally coordinated VO_4 species (51, 52). Notably, there is no peak near 1000 cm^{-1} corresponding to the stretching vibrations of V=O bonds for isolated vanadyl species such as are observed for vanadia dispersed on Al_2O_3, SiO_2, TiO_2, and ZrO_2 (13, 14, 45). At a loading of 20 wt%, new features appear at 380 and 860 cm^{-1} together with the peak at 825 cm^{-1}, which increases in intensity. Increasing the loading further to 25 and 30 wt% increases the intensity of the bands at 380 and 860 cm^{-1} and leads to the appearance of a broad band at 950 cm^{-1}. The peaks at 380 and 860 cm^{-1} and the increase in the band intensity at 825 cm^{-1} are attributed to $Mg_3(VO_4)_2$, whereas

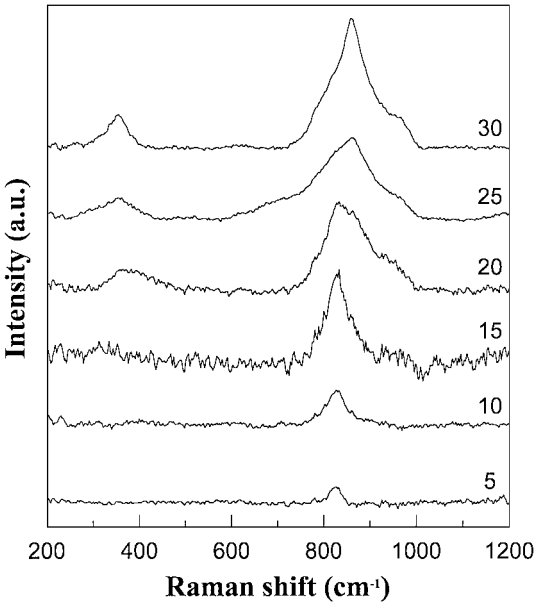

FIG. 2. Raman spectra of V–Mg–O catalysts as a function of V_2O_5 loading.

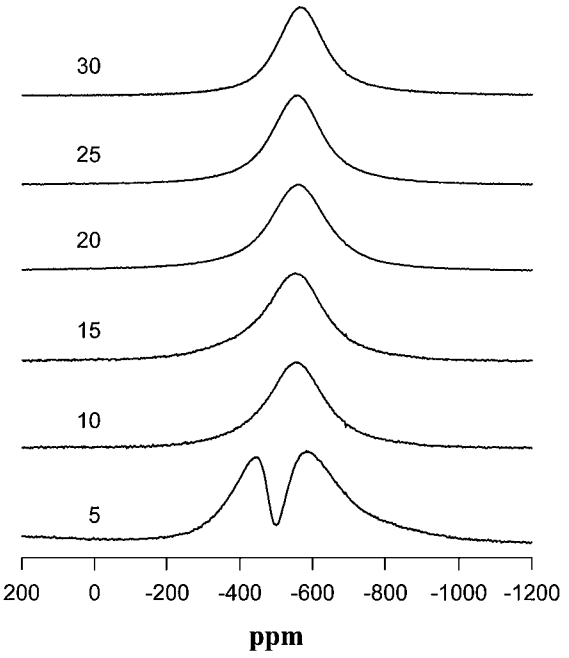

FIG. 3. Static solid-state ^{51}V NMR spectra of V–Mg–O catalysts as a function of V_2O_5 loading.

the appearance of the band at 950 cm^{-1} is attributed to $Mg_2(V_2O_7)$ (22, 24, 27, 28, 53–55). The Raman spectrum of bulk $Mg_2(V_2O_7)$ exhibits a very intense peak at 902 cm^{-1} (55). This peak may be present in the spectrum for the 30 wt% V_2O_5 sample shown in Fig. 2 as part of the broad band observed between 800 and 1000 cm^{-1}. Raman peaks for V_2O_5 were not observed at any vanadia loading.

Static solid-state ^{51}V NMR spectra of the catalysts are presented in Fig. 3. With the exception of the 5 wt% V_2O_5, all of the samples show an isotropic broad peak centered at ca. −560 ppm. The shape and chemical shift of this peak are very similar to that for pure $Mg_3(VO_4)_2$ (19, 56, 57). In the case of the 5 wt% V/MgO sample, two peaks are observed at ca. −450 and −580 ppm, which are also located in the range of chemical shifts for vanadium atoms in a distorted tetrahedral environment (52, 53). Peaks at −480 and −570 ppm have been reported previously in V–Mg–O samples with vanadia loadings below 10 wt% V_2O_5 (57, 58). The first peak is attributed to isolated, tetrahedrally coordinated vanadium ions and the second peak is attributed to tetrahedrally coordinated vanadium atoms in which the V–V distance is shorter than that for the first peak.

Temperature-programmed reduction (TPR) traces are shown in Fig. 4. For the samples with low loading, two peaks are observed at 640 and 813 K, suggesting the presence of two different types of vanadium species (15, 28, 59, 60). With increasing vanadia loading, the first peak diminishes gradually and the maximum of the second peak shifts from 813 to 853 K. The TPR traces in Fig. 4 are similar to those reported previously for V–Mg–O prepared by aqueous impregnation (15, 25, 59). Based on the data obtained from Raman spectroscopy and ^{51}V NMR, the TPR peak at 640 K can be assigned to the reduction of tetrahedrally coordinated V^{5+} in isolated VO_4^{2-} species. The peak at 813–853 K can be assigned to the reduction of V^{5+} in small domains

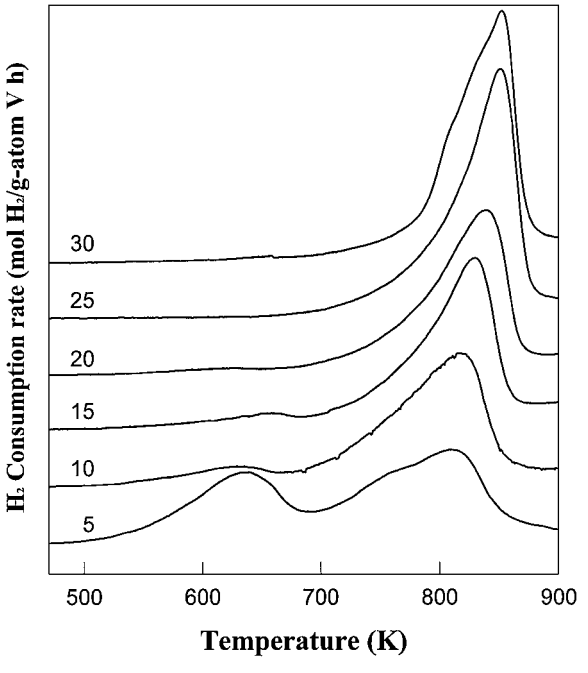

FIG. 4. TPR profiles for V–Mg–O catalysts as a function of V_2O_5 loading.

TABLE 1

Surface Area, Nominal Loading, Apparent Surface Density of VO_x, and UV–visible Absorption Edge Energy for V–Mg–O Catalysts

Sample	Nominal wt% of V_2O_5	Surface area ($m^2\ g^{-1}$)	Apparent surface density of VO_x (nm^{-1})	Absorption edge energy (eV)
5 V–Mg–O	5	307	1.1	3.05
10 V–Mg–O	10	299	2.2	2.88
15 V–Mg–O	15	280	3.5	2.89
20 V–Mg–O	20	256	5.2	2.90
25 V–Mg–O	25	227	7.3	2.94
30 V–Mg–O	30	187	10.6	2.95

of $Mg_3(VO_4)_2$. It is notable that as the loading of vanadia increases and the sizes of the $Mg_3(VO_4)_2$ domains grow, the vanadium cations become more difficult to reduce. Consistent with this, the peak temperature for reduction of bulk $Mg_3(VO_4)_2$ is 903 K.

The absorption band edge energies, based on Tauc's law (61, 62), were determined from UV–visible spectra and are reported in Table 1. The band edge energy is 3.05 eV for the catalyst containing 5 wt% V_2O_5 and decreases to about 2.90 eV as the loading of vanadia is increased to 20 wt%. Above this level, the edge energy rises slightly, to about 2.95 eV. The values of the band edge energies are characteristic of those for isolated tetrahedrally coordinated species. For example $Mg_3(VO_4)_2$ has a band edge of 3.34 eV (63) and $O{=}V(OSi(O^tBu)_3)_3$ has a band edge energy of 3.48 eV (64). By contrast, V_2O_5 in which vanadium is octahedrally coordinated has a band edge energy of 2.21 eV (65).

The structural analyses presented above indicate that at a vanadia loading of 5 wt% (1.1 VO_x/nm^2) V atoms are present at the surface of MgO as isolated VO_4 species in distorted tetrahedral coordination. These species are characterized by the Raman band at 825 cm^{-1}, the ^{51}V NMR shift of −480 ppm, and the UV–visible absorption band edge energy of 3.05 eV. Temperature-programmed reduction of this species in H_2 produces a peak at 640 K. For vanadia loadings above 10 wt% (2.2 VO_x/nm^2), small domains of $Mg_3(VO_4)_2$ are formed. The presence of this phase is noted by the appearance of Raman bands at 380 and 860 cm^{-1} and a ^{51}V NMR resonance at −560 ppm. The formation of small domains of $Mg_2V_2O_7$ is suggested by the appearance of a Raman band at 950 cm^{-1}. The absence of any evidence for such a phase in the ^{51}V NMR spectra is not surprising, since the v1 peak for the α and β phases of $Mg_2V_2O_7$ overlaps the single peak for $Mg_3(VO_4)_2$ and the v2 peak for $Mg_2V_2O_7$ would not be observable for small quantities of this phase (56). With increasing loading, the domains of magnesium vanadate become progressively more difficult to reduce and the peak temperature for their reduction shifts from 813 to 853 K, but remains less than that for bulk $Mg_3(VO_4)_2$, 903 K.

Catalyst Activity and Selectivity

Figure 5 shows an example of the dependencies for propene, CO, and CO_2 formation rates on the ratio of catalyst mass to feed flow rate. For a fixed catalyst mass, the rates of formation of all products decreased with decreasing feed flow rate, this effect being most severe for the rate of propene formation. The total rate of propane consumption also decreased with decreasing feed flow rate as a consequence of inhibition by water vapor (66). The decline in propene selectivity with decreasing feed flow rate, seen in Fig. 5, is due to the secondary combustion of propene (13, 14, 66, 67).

Initial rates of propane ODH are reported in Fig. 6 as a function of vanadium surface density at different reaction temperatures. The solid points are for catalysts with different weight loadings of V_2O_5 calcined at 550 K, whereas the open points are for a sample containing 15 wt% calcined at 823, 923, and 1073 K to achieve progressively higher apparent vanadia surface densities. As shown in Fig. 6A, propene formation rates normalized per V atom increased up to 3.5 VO_x/nm^2 and then decreased with further increase in vanadium loading irrespective of whether the increase in apparent surface density was achieved by increasing the

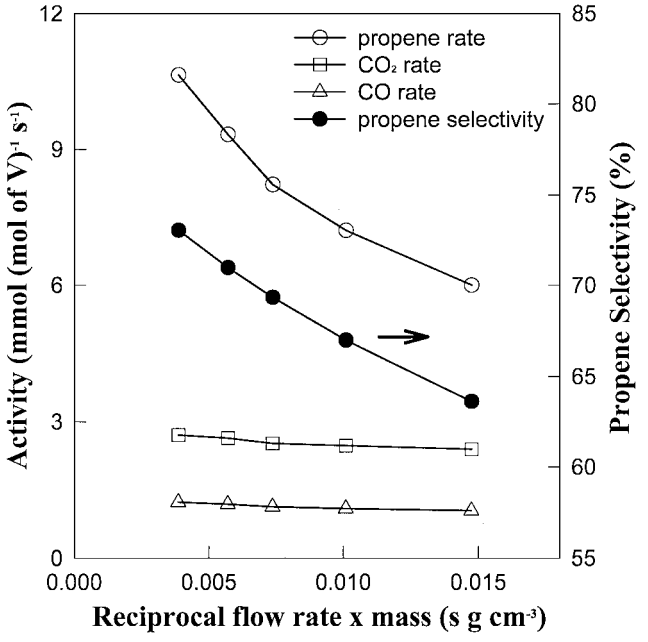

FIG. 5. Rates of propene, CO, and CO_2 formation and propene selectivity as functions of the reciprocal of the flow rate per unit of catalyst mass for 25 wt% V–Mg–O. Reaction conditions: temperature, 773 K; feed flow rate, $C_3H_8/He/N_2/O_2$ at 25/199/2/9 cm^3/min; pressure, 1 atm; catalyst mass, 0.015 g.

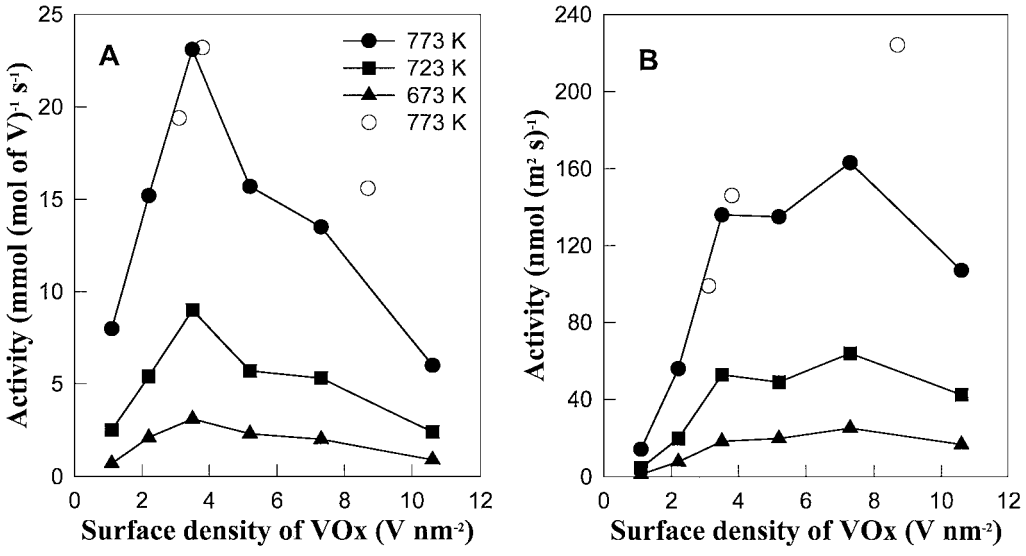

FIG. 6. Effects of apparent VO_x surface density and reaction temperature on the initial rate of propene formation: (A) normalized per V atom and (B) normalized per unit surface area of the catalyst.

weight loading of V_2O_5 or the calcination temperature. The only exception to this general trend is for the sample containing 15 wt% V_2O_5 calcined at 1073 K, which exhibits a significantly higher activity than would be expected. The trend of activity with apparent vanadia surface density is similar to that reported previously for V–Mg–O (19, 21) and for VO_x/ZrO_2 and VO_x/Al_2O_3 (13, 14). The decrease in specific activity beyond the maximum has been ascribed to the formation of multilayers of the active form of vanadia, with the consequence that V atoms lying below the surface are inaccessible. Figure 6B supports this interpretation. The rate of propene formation per unit surface area of the catalysts increases rapidly with increasing V surface density up to about 3.5 VO_x/nm^2, but then reaches a plateau. Also consistent with the proposed explanation is the recognition that the surface density of VO_x for $Mg_3(VO_4)_2$ is approximately 4.2 VO_x/nm^2. Here, too, the behavior of the catalysts appears to be independent of the means of achieving the increase in apparent vanadia surface density, with the exception of the data point for the sample containing 15 wt% V_2O_5, calcined at 1073 K.

Plots of propene selectivity at zero propane conversion are shown in Fig. 7 as a function of the apparent vanadium surface density for different reaction temperatures. At 673 K, the selectivity to propene increased up to a vanadium surface density of about 7.3 VO_x/nm^2, after which it remained almost constant at about 80%. Increasing the reaction temperature increased the propene selectivity only slightly. The observed trend in selectivity with the apparent surface density of VO_x is very similar to that reported previously for vanadia dispersed on MgO (25, 30), ZrO_2 (13, 14, 45), and Al_2O_3 (14). The data in Fig. 7 also demonstrate that there is no effect of the means by which an increase in the apparent surface density of vanadia is achieved.

The effects of catalyst structure on catalyst activity and selectivity are best discussed in terms of Scheme 1. Propane can undergo either oxidative dehydrogenation to form propene or combustion to form CO_x, reactions 1 and 2, whereas propene can undergo combustion to CO_x, reaction 3. If the conversion of oxygen is low, then the rates of

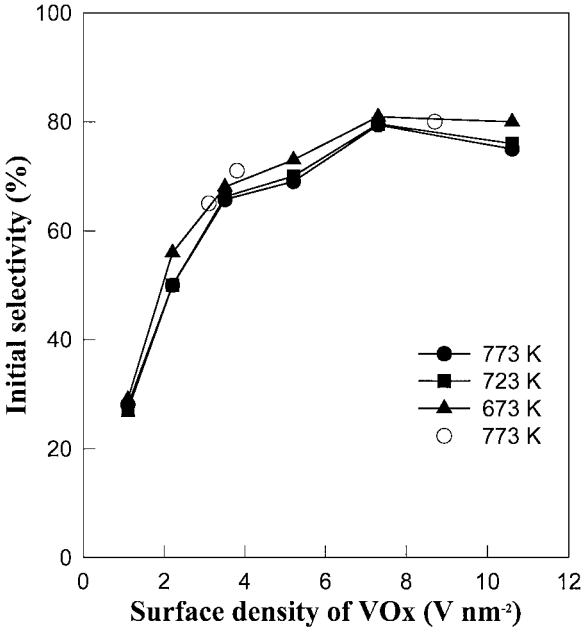

FIG. 7. Dependence of propene selectivity on the apparent surface density of VO_x and reaction temperature.

these three processes can be described by the pseudo-first-order rate coefficients, k_1, k_2, and k_3 (13, 14).

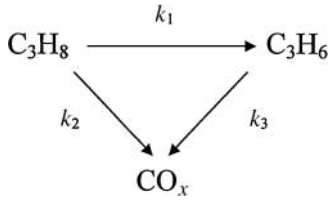

SCHEME 1

The value of k_1, expressed per unit of catalyst surface area, is shown in Fig. 8 as a function of the apparent surface density of vanadia for different temperatures. For each temperature, the value of k_1 increases rapidly up to about 4.0 VO_x/nm^2, remains constant, and then decreases slightly. The activation energy for propane ODH is 102 kJ/mol for the 5 wt% catalyst and decreases to about 80 kJ/mol for the catalysts containing 10–30 wt% V_2O_5. Taken in light of the structural characterization discussed above, the increase in k_1 seen in Fig. 8 up to a vanadia surface density of about 4 VO_x/nm^2 suggests that isolated VO_4^{2-} units are not as active as those present at the surface of $Mg_3(VO_4)_2$. The vanadia surface density at which the plateau in k_1 and the apparent activation energy are reached is also consistent with this interpretation. Based on the (100) surface of $Mg_3(VO_4)_2$, the surface density of VO_4^{2-} units is estimated to be 4.2 VO_x/nm^2. Thus, the data reported here support the view that the most active species for propane ODH are VO_4^{2-} species existing in a surface structure that is essentially identical to that present in $Mg_3(VO_4)_2$. This conclusion is identical to that reached by Pantazidis and Miradatos for V–Mg–O catalysts prepared by conventional means (30).

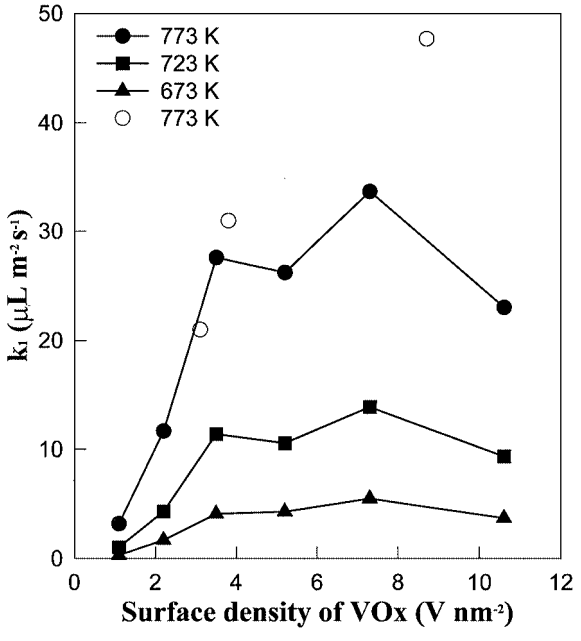

FIG. 8. Dependence of k_1 on the apparent VO_x surface density and reaction temperatures.

An alternate view of the active center in V–Mg–O catalysts has been proposed by Kung and coworkers (21) and López Nieto and coworkers (22–25). Both groups concluded that isolated VO_4^{2-} units distributed at the surface of MgO exhibit the highest activity for propane ODH. The latter set of authors based their conclusion on the observation that with increasing V_2O_5 loading, maxima were observed at 20 wt% in both the rate of propane ODH at 773 K and the area of the TPR peak centered at 633 K. Since the TPR peak at 633 K had been assigned to the reduction of isolated VO_4^{2-} species, it was deduced that these are the active centers for propane ODH. Several observations suggest that this conclusion needs to be reexamined. First, in Refs. (23, 25), the authors report a maximum in the appearance of $Mg_3(VO_4)_2$, with increasing V_2O_5 loading occurring at 20 wt%; however, no mention is made of the relationship of this feature to the corresponding maximum in catalyst activity. Second, we report here that the activity of V–Mg–O catalysts continues to increase with increasing V_2O_5 loading even when there is no evidence, by either Raman or NMR spectroscopy, or by H_2 TPR, for isolated VO_4^{2-} species. In fact, all of the evidence suggests that the only V-containing phase is $Mg_3(VO_4)_2$. Third, the maximum in activity with V_2O_5 loading reported by López Nieto and coworkers (23, 25) could quite possibly be due to the formation of bulk $Mg_3(VO_4)_2$. This suggestion is reached by recognizing that the decrease in the ODH activity per unit surface area reported by López Nieto and coworkers occurs for catalysts having apparent vanadia surface areas in the range of 10–73 VO_x/nm^2. These apparent surface densities are considerably higher than those used in the present study and are within a range where it is not unreasonable to expect the formation of larger crystallites of $Mg_3(VO_4)_2$. To assess how the area-based activity of bulk $Mg_3(VO_4)_2$ compares with that of the most active catalysts reported here, we measured the zero-conversion activity of the bulk material for propene formation at 773 K and the same feed composition used throughout our work. The result is that bulk $Mg_3(VO_4)_2$ (11 m^2/g) has an activity of 3.9 $nmol/m^2 \cdot s$, whereas V–Mg–O catalysts containing 15 and 25 wt% of V_2O_5 have activities of 136 and 163 $nmol/m^2 \cdot s$, respectively. Thus, it appears likely that as the proportion of bulk $Mg_3(VO_4)_2$ increases, the area-based activity of the catalyst will decrease. We conclude, therefore, that the most active V–Mg–O catalysts are those that contain very small domains of a $Mg_3(VO_2)_4$ on the surface of MgO rather than crystallites of bulk $Mg_3(VO_2)_4$. The XRD data presented in Fig. 1 suggest that these domains are not very crystalline.

The one anomaly in the data shown in Fig. 8 is for the sample containing 15 wt% V_2O_5 that had been calcined at 1073 K, which exhibits a significantly higher value of k_1 than would be expected for the corresponding apparent surface density of vanadia. No explanation can be offered at this time for this discrepancy, but its occurrence suggests that the activity of V–Mg–O catalysts can depend on the nature of the precursor used to introduce V atoms and on the time–temperature history of the catalyst pretreatment.

Several authors have suggested that the reducibility of vanadia-containing catalysts is a good predictor of their activity for propane ODH (15, 22, 25). This conclusion has been based on the observation of an inverse correlation between either the peak temperature or the onset temperature for vanadia reduction by H_2 for vanadia supported on different oxides. The data presented in Figs. 4 and 6 show, however, that the V–Mg–O catalysts investigated in this study exhibit an increase in ODH activity with increasing peak temperature for TPR by H_2. Based on this observation, we suggest that a low value of the peak temperature for vanadia reduction by H_2 would not be an appropriate predictor for the propane ODH activity of V–Mg–O catalysts. The reason for this is that as the vanadia loading increases, the O atoms associated with the $Mg_3(VO_4)_2$ domains become less accessible because an increasing number of them lie below the oxide surface. An increase in the degree of crystallinity of the $Mg_3(VO_4)_2$ may also contribute to the rise in the peak temperature for reduction. Consistent with this it is observed that the peak temperature for the reduction of bulk $Mg_3(VO_4)_2$ (903 K) is significantly higher than that for $Mg_3(VO_4)_2$ supported on MgO (813–853 K). It has recently been proposed that a better metric for ODH activity of vanadia-containing catalysts is the magnitude of the UV–visible absorption edge energy, since the initial step in propane ODH is hypothesized to involve one-electron reduction of two closely spaced V^{5+} centers (68). Figure 9 shows that the propane ODH activity of the V–Mg–O catalysts increases with a decrease in the absorption edge energy, indicating that ODH activity correlates with the ease of electron transfer from the O anions surrounding a V^{5+} cation.

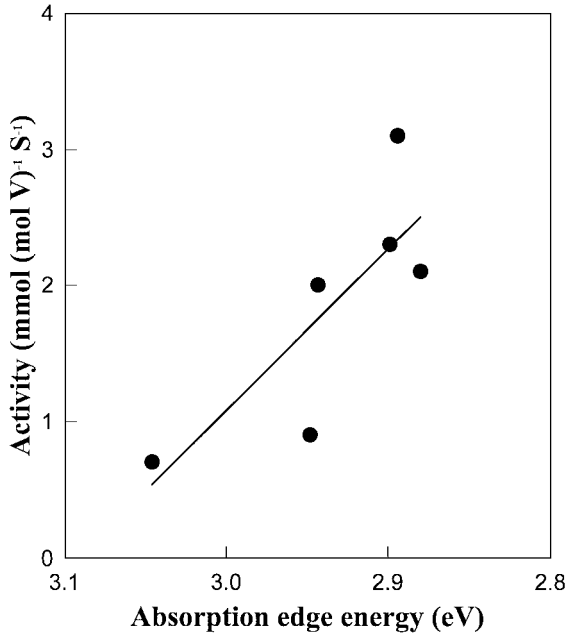

FIG. 10. Dependence of k_2/k_1 (A) and k_3/k_1 (B) on the apparent VO_x surface density and reaction temperature

Figures 10A and 10B show the effects of the apparent surface density of vanadia on the values of k_2/k_1 and k_3/k_1, respectively. The value of k_2/k_1 decreases rapidly with rising

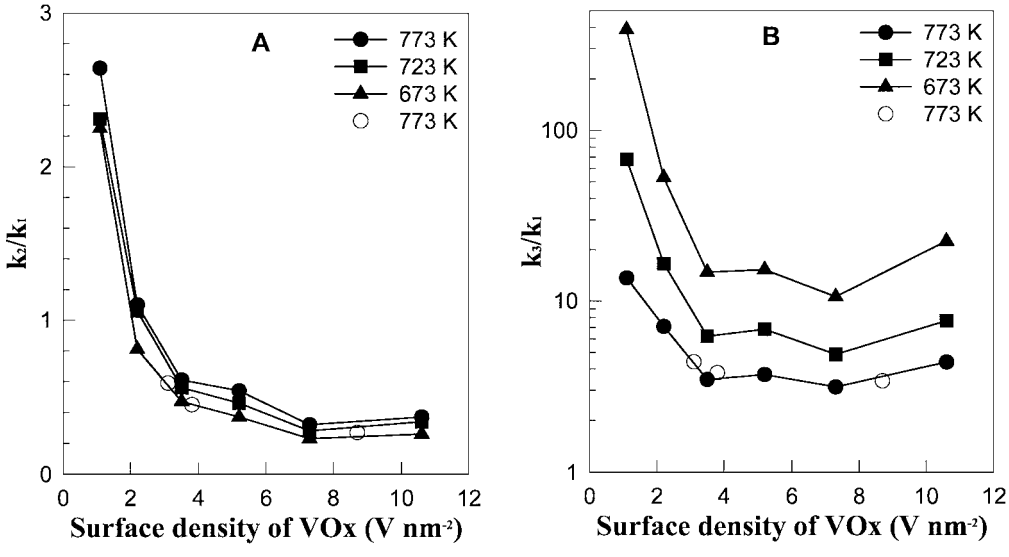

FIG. 9. Dependence of the rate of propene formation per V atom on the UV–visible absorption edge energy. Reaction conditions: temperature, 673 K; feed flow rate, $C_3H_8/He/N_2/O_2$ at 25/199/2/9 cm^3/min; pressure, 1 atm; catalyst mass, 0.015 g.

TABLE 2

Comparison of Activity and Selectivity for Vanadium-Supported MgO Catalysts[a]

Ref.	Vanadium source	Support	V_2O_5 (wt%)	Surface area (m^2/g)	VO_x density[b] (nm^{-2})	Propane conversion (%)	Propene selectivity (%)	Activity	
								mmol/g · h	nmol/m^2 · s
This work	$OV(O^tBu)_3$	MgO	15	280	3.5	0	66	137	136
						10.2	52	57.2	56.7
This work	$OV(O^tBu)_3$	MgO	25	227	7.3	0	79	133	163
						9.2	64	59.4	72.6
15	NH_4VO_3	MgO	4.7	101	3.1	4.3	31	24.3	66.8
22	$(NH_4)_2VO(C_2O_4)$	MgC_2O_4	19.7	136	9.6	0	70	85.5	174.9
18	NH_4VO_3	$Mg(OH)_2$	23	81	11	0	60	NA[c]	NA[c]
17	NH_4VO_3	MgO	3.85	98.2	2.6	13	33	NA[c]	NA[c]
29	NH_4VO_3	MgO	24	41.5	38	10	49	18.4	122.7
30	NH_4VO_3	MgO	23.7	74	21	13	60	13.0	48.7

[a] Reaction conditions: temperature, 773 K; feed flow rate, $C_3H_8/He/N_2/O_2$ at 25/199/2/9 cm^3 min^{-1}; pressure, 1 atm; catalyst mass, 0.015 g.

[b] The apparent surface density calculated assuming all of the VO_x present is on the surface.

[c] NA, Not applicable. Authors do not provide the necessary information to enable conversion of the reported activity to the reaction conditions used in this study.

vanadia surface density but approaches a plateau above a density of 4 VO_x/nm^2. A similar pattern is seen for k_3/k_1. The open points in this figure are for a sample containing 15 wt% V_2O_5 calcined at 823, 923, and 1073 K in order to achieve higher apparent surface densities of vanadia. It is evident that identical values of k_2/k_1 and k_3/k_1 are obtained irrespective of how a given value of the apparent surface density of vanadia is achieved. The appearance of a plateau in plots of k_2/k_1 and k_3/k_1 can be ascribed to the formation of a monolayer of $Mg_3(VO_4)_2$. The decrease in the values of k_2/k_1 and k_3/k_1 observed at apparent surface densities below 4 VO_x/nm^2 can be ascribed to changes in the reactivity of oxygen at the surface of the catalyst. The TPR traces presented in Fig. 3 show that for temperatures between 673 and 773 K, the reducibility of the catalyst decreases with increasing vanadia loading. This trend is particularly evident for vanadia loadings between 5 and 15 wt% and suggests that the oxygen associated with isolated VO_4^{2-} species is much more readily available for combustion of propane and propene than oxygen associated with domains of $Mg_3(VO_4)_2$. Consistent with this we note that the peak temperature for the reduction of bulk $Mg_3(VO_4)_2$ is higher than that for 30 V–Mg–O and, correspondingly, so are the values of k_2/k_1 and k_3/k_1. We note that a similar trend has been reported for the ODH of butane over various metal vanadate catalysts (5).

Finally, it is interesting to compare the activity and selectivity of the catalysts prepared in this study with those reported previously for V–Mg–O catalysts prepared by conventional means (15, 17, 18, 22, 29, 30). Table 2 lists the activity and selectivity of the most active catalysts reported here, together with the activities and selectivities of V–Mg–O described in the literature. In all cases, the ODH of propane was investigated at 773 K. Since different authors used different partial pressures of propane, the rates reported were corrected to a propane partial pressure in the feed of 11 kPa, assuming a first-order dependence of the rate of propane ODH on propane partial pressure. No adjustment for the partial pressure of oxygen was made, since the dependence on oxygen is typically zero order (18). The data in Table 2 show that the catalysts prepared in this study exhibit activities on an area basis that are comparable to those prepared from other inorganic precursors when compared at the same level of propane conversion. It is also noted that the propane selectivity of our catalysts at zero propane conversion is as good or better than that for catalysts prepared by conventional approaches. Most notable, however, is the much higher activity of the catalysts reported here when rates are expressed on the basis of catalyst mass, which is a direct consequence of the higher surface area of the support used in this study.

CONCLUSIONS

A series of V–Mg–O catalysts have been prepared by impregnation of $OV(O^tBu)_3$ onto high-surface-area MgO. After calcination at 823 K, these catalysts have surface areas ranging from 307 m^2/g for 5 wt% V–Mg–O to 187 m^2/g for 30 wt% V–Mg–O. Structural characterization of the dispersed vanadium shows evidence for isolated VO_4^{2-} anions for V_2O_5 loadings below 5 wt%. With increasing V_2O_5 loading, small domains of $Mg_3(VO_4)_2$ are observed, but there is no evidence for either polyvanadate species or V_2O_5 domains. The area-based activities of the catalysts prepared in this study were significantly higher than those of V–Mg–O catalysts prepared by conventional methods involving aqueous impregnation of MgO, whereas the propene selectivties were comparable to or slightly better than those previously reported. The rate coefficient for ODH, k_1, increased with increasing apparent surface density of V_2O_5,

reaching a plateau at a surface density of about 4 VO_x/nm^2, which corresponds closely to the surface density of VO_x in $Mg_3(VO_4)_2$. Correspondingly, the apparent activation energy for propane ODH decreased from 102 kJ/mol for the lowest surface loading of V_2O_5 and reached a plateau of 80 kJ/mol at a surface loading of about 4 VO_x/nm^2. Consideration of the structural characterization data indicates that the most active form of the catalyst is that in which the surface of the MgO support is covered by small domains of $Mg_3(VO_4)_2$. The formation of bulk crystallites of $Mg_3(VO_4)_2$ is undesirable, since it is found that the area-based activity of the pure phase is approximately 40 times lower than that of the domains of $Mg_3(VO_4)_2$ formed on the surface of MgO. The values of k_2/k_1 and k_3/k_1 decrease with increasing V_2O_5 surface density but reach a nearly constant value for surface densities above 4 VO_x/nm^2. These trends show that the activities of V–Mg–O catalysts for propane and propene combustion relative to propane ODH decline with increasing surface loading of V_2O_5. The value of k_2/k_1 changes very little with increasing temperature, whereas the value of k_3/k_1 decreases. These trends indicate that the apparent activation energies for propane ODH and combustion are virtually identical, but that the activation energy for propane ODH is higher than that for propene combustion.

ACKNOWLEDGMENTS

The authors acknowledge P. F. Mulato and J. A. Reimer for assistance in acquiring the NMR data and K. Chen for assistance in acquiring the temperature-programmed reduction and UV–visible data reported here. This work was supported by the Director, Office of Basic Energy Sciences, Chemical Sciences Division, of the U.S. Department of Energy through Grant DE-AC03-76SF00098.

REFERENCES

1. Kung, H. H., *Adv. Catal.* **40**, 1 (1994).
2. Mamedov, E. A., and Cortes Corberan, V., *Appl. Catal. A* **127**, 1 (1995).
3. Cavani, F., and Trifiro, F., *Catal. Today* **24**, 307 (1995).
4. Albonetti, S., Cavani, F., and Trifiro, F., *Catal. Rev.–Sci. Eng.* **38**, 413 (1996).
5. Kung, H. H., and Kung, M. C., *Appl. Catal. A* **157**, 105 (1997).
6. Blasco, T., and López Nieto, J. M., *Appl. Catal. A* **157**, 117 (1997).
7. Kijenski, J., Baiker, A., Glinski, M., Dollenmeier, P., and Wokaun, A., *J. Catal.* **101**, 1 (1986).
8. Deo, G., and Wachs, I., *J. Catal.* **129**, 307 (1991).
9. Vedrine, J. C., Millet, J. M. M., and Volta, J.-C., *Catal. Today* **32**, 115 (1996).
10. Wachs, I., and Wechuysen, B. M., *Appl. Catal.* **157**, 67 (1997).
11. Gryzbowska-Swierkosz, B., *Appl. Catal.* **157**, 409 (1997).
12. Puglisi, M., Arena, F., Frusteri, F., Sokolovskii, V., and Parmaliana, A., *Catal. Lett.* **41**, 41 (1998).
13. Khodakov, A., Yang, J., Su, S., Iglesia, E., and Bell, A. T., *J. Catal.* **177**, 343 (1998).
14. Khodakov, A., Olthof, B., Bell, A. T., and Iglesia, E., *J. Catal.* **181**, 205 (1999).
15. Arena, F., Frusteri, F., and Parmaliana, A., *Catal. Lett.* **60**, 59 (1999).
16. Viparelli, P., Ciambelli, P., Lisi, L., Ruoppolo, G., Russo, G., and Volta, J. C., *Appl. Catal. A* **184**, 291 (1999).
17. Lemoninou, A. A., Nalbandian, L., and Vasalos, I. A., *Catal. Today* **61**, 333 (2000).
18. Chaar, M. A., Patel, D., and Kung, H. H., *J. Catal.* **109**, 463 (1988).
19. Siew Hew Sam, D., Soenen, V., and Volta, J. C., *J. Catal.* **123**, 417 (1990).
20. Guerrero-Ruiz, A., Rodriguez-Ramos, I., Fierro, J. C., Soenen, V., Herrmann, J. M., and Volta, J. C., *in* "New Developments in Selective Oxidation by Heterogenous Catalysis" (P. Ruiz and B. Delmon, Eds.), Studies in Surface Science and Catalysis, Vol. 72, p. 203. Elsevier, Amsterdam, 1992.
21. Michalakos, P. M., Kung, M. C., and Kung, H. H., *J. Catal.* **140**, 226 (1993).
22. Corma, A., López Nieto, J. M., and Paredes, N., *J. Catal.* **144**, 425 (1993).
23. Corma, A., López Nieto, J. M., Paredes, N., and Perez, M., *Appl. Catal. A* **97**, 159 (1993).
24. Corma, A., López Nieto, J. M., Paredes, N., and Perez, M., *Appl. Catal. A* **104**, 161 (1993).
25. Corma, A., López Nieto, Paredes, N., Dejoz, A., and Vasquez, I., *in* "New Developments in Selective Oxidation II" (C. Cortés Corberán and S. Vic Bellón, Eds.), Studies in Surface Science and Catalysis, Vol. 82, p. 113. Elsevier, Amsterdam, 1994.
26. Gao, X., Ruiz, P., Xin, Q., Guo, X., and Delmon, B., *Catal. Lett.* **23**, 321 (1994).
27. Gao, X., Ruiz, P., Xin, Q., Guo, X., and Delmon, B., *J. Catal.* **148**, 56 (1994).
28. Concepción, P., López Nieto, J. M., and Perez-Pariente, J., *J. Mol. Catal. A* **97**, 173 (1995).
29. Valenzuela, R. X., Mamedov, E. A., and Vasalos, I. A., *Reac. Kinet. Catal. Lett.* **55**, 213 (1995).
30. Pantazidis, A., and Mirodatos, C., *in* "Heterogeneous Hydrocarbon Oxidation" (B. K. Warren and S. T. Oyama, Eds.), ACS Symposium Series, Vol. 638, p. 207. Am. Chem. Soc., Washington, DC, 1996.
31. Pantazidis, A., Auroux, A., Herrmann, J.-M., and Mirodatos, C., *Catal. Today* **32**, 81 (1996).
32. Pantazidis, A., and Miordatos, C., *in* "Proceedings, 11th International Congress on Catalysis, Baltimore, 1996" (J. W. Hightower, W. N. Delgass, E. Iglesia, and A. T. Bell, Eds.), p. 1029. Elsevier, Amsterdam, 1994.
33. Michaels, J. N., Stern, D. L., and Graselli, R. K., *Catal. Lett.* **42**, 135 (1996).
34. Stern, D. L., Michaels, J. N., De Caul, L., and Graselli, R. K., *Appl. Catal. A* **153**, 21 (1997).
35. Pantazidis, A., Burrows, A., Kiely, C. J., and Mirodatos, C., *J. Catal.* **177**, 325 (1998).
36. Oganowski, W., Hanuza, J., Kepinski, L., Mista, W., Maczka, M., Wyrostek, A., and Bukowski, Z., *J. Mol. Catal. A* **136**, 91 (1998).
37. López Nieto, J. M., Soler, J., Concepción, P., Herguido, J., Menéndez, M., and Santamaría, J., *J. Catal.* **185**, 324 (1999).
38. Jiang, J., Decker, S., Mohs, C., and Klabunde, K. J., *J. Catal.* **180**, 24 (1998).
39. Klabunde, K. J., Stark, J., Koper, O., Mohs, C., Park, D. G., Decker, S., Jiang, Y., Lagadic, I., and Zhang, D., *J. Phys. Chem.* **100**, 12142 (1996).
40. Utamapanya, S., Klabunde, K. J., and Schlup, J. R., *Chem. Mater.* **3**, 175 (1991).
41. Coles, M. P., Lugmair, C. G., Terry, K. W., and Tilley, T. D., *Chem. Mater.* **12**, 122 (2000).
42. Rulkens, R., Male, J. L., Terry, K. W., Olthof, B., Khodakov, A., Bell, A. T., Iglesia, E., and Tilley, T. D., *Chem. Mater.* **11**, 2966 (1999).
43. Terry, K. W., Lugmair, C. G., and Tilley, T. D., *J. Am. Chem. Soc.* **119**, 9745 (1997).
44. Rulkens, R., and Tilley, T. D., *J. Am. Chem. Soc.* **120**, 9959 (1998).
45. Male, J. L., Niessen, H. G., Bell, A. T., and Tilley, T. D., *J. Catal.* **194**, 432 (2000).
46. Prandtl, W., and Hess, L. Z., *Z. Anorg. Allg. Chem.* **82**, 103 (1913).
47. Glinski, M., *Appl. Catal. A* **164**, 205 (1997).

48. Ding, Y., Zhang, G., Wu, H., Hai, B., Wang, L., and Qian, Y., *Chem. Mater.* **13**, 435 (2001).
49. Burraws, A., Kiely, C. J., Perregaard, J., Hojlund-Nielsen, P. E., Vorbeck, G., Calvino, J. J., and Lopez-Cartes, C., *Catal. Lett.* **57**, 121 (1999).
50. Tellez, C., Abon, M., Dalmon, J. A., Mirodatos, C., and Santamaria, J., *J. Catal.* **195**, 113 (2000).
51. Deo, G., and Wachs, I. E., *J. Phys. Chem.* **95**, 5889 (1991).
52. Yurdakoc, M. K., Haffner, R., and Honicke, D., *Mater. Chem. Phys.* **44**, 273 (1996).
53. Valenzuela, R. X., and Cortés Corberán, V., *Top. Catal.* **11/12**, 153 (2000).
54. Hanuza, J., Jezowska-Trzebiatowska, B., and Oganowski, W., *J. Mol. Catal.* **29**, 109 (1985).
55. Busca, G., Ricchiardi, G., Sam, D. S. H., and Volta, S.-C., *J. Chem. Soc. Faraday Trans*. **90**, 1161 (1994).
56. Occelli, M. L., Maxwell, R. S., and Eckert, H., *J. Catal.* **137**, 36 (1992).
57. Lapina, O. B., Simakov, A. V., Mastikhin, V. M., Veniaminov, S. A., and Shubin, A. A., *J. Mol. Catal.* **50**, 55 (1989).
58. Lapina, O. B., Mastikhin, V. M., Shubin, A. A., Krasilnokov, V. N., and Zamaraev, K. I., *Prog. Nucl. Magn. Reson. Spectrosc.* **24**, 457 (1992).
59. Arena, F., Frusteri, F., and Parmaliana, A., *Appl. Catal. A* **176**, 189 (1999).
60. Blasco, T., López Nieto, J. M., Dejoz, A., and Vazquez, M. I., *J. Catal.* **157**, 271 (1995).
61. Tauc, J., *in* "Amorphous and Liquid Semiconductors" (J. Tauc, Ed.), p. 159. Plenum, London, 1974.
62. Barton, D. G., Shtein, M., Wilson, R. D., Soled, S. L., and Iglesia, E., *J. Phys. Chem. B* **103**, 630 (1999).
63. Gao, X., Bare, S. R., Weckhuysen, B. M., and Wachs, I. E., *J. Phys. Chem. B* **102**, 10842 (1998).
64. Rulkens, R., Male, J. L., Terry, K. W., Olthof, B., Khodakov, A., Bell, A. T., Iglesia, E., and Tilley, T. D., *Chem. Mater*. **11**, 2966 (1999).
65. Kenny, N., Kanneworf, C. R., and Whitmore, D. H., *J. Phys. Chem. Solids* **27**, 1237 (1966).
66. Chen, K., Khodakov, A., Yang, J., Bell, A. T., and Iglesia, E., *J. Catal.* **186**, 325 (1999).
67. Chen, K., Bell, A. T., and Iglesia, E., *J. Phys. Chem. B* **104**, 1292 (2000).
68. Chen, K., Iglesia, E., and Bell, A. T., submitted for publication.